Pharmaceutical Research, Vol. 27, No. 4, April 2010 (© 2010)
DOI: 10.1007/s11095-010-0072-3

Research Paper

Prostate Cancer-Targeted Imaging Using Magnetofluorescent Polymeric Nanoparticles Functionalized with Bombesin

Chang-Moon Lee,[1,2,3] Hwan-Jeong Jeong,[1,2,3,4] Su-Jin Cheong,[1,2,3] Eun-Mi Kim,[1,2,3] Dong Wook Kim,[1,2,3] Seok Tae Lim,[1,2,3] and Myung-Hee Sohn[1,2,3]

Received November 18, 2009; accepted January 13, 2010; published online February 25, 2010

Purpose. In this work, the aim was to prepare and characterize a magnetofluorescent polymeric nanoparticle for prostate cancer imaging *in vivo*.
Methods. Glycol chitosan (GC) was chemically modified with *N*-acetyl histidine (NAHis) as a hydrophobic moiety, and bombesin (BBN) was conjugated to the hydrophobically modified GC for use in targeting gastric-releasing peptide receptors (GRPR) overexpressed in prostate cancer cells. NAHis-GC conjugates were labeled with the near-infrared (NIR) fluorophore Cy5.5 (C-NAHis-GC conjugate).
Results. BBN-conjugated C-NAHis-GC nanoparticles (BC-NAHis-GC nanoparticles) showed significantly higher binding to the PC3 cell surface than nanoparticles without BBN, and the cellular binding was clearly inhibited by BBN. The tumor-to-muscle ratios of C- and BC-NAHis-GC nanoparticles were 2.26±0.66 and 5.37±0.43, respectively. The tumor accumulation of BC-NAHis-GC nanoparticles was clearly reduced by co-injection of BBN. Further, iron oxide nanoparticles (IO) were loaded into BC-NAHis-GC nanoparticles to investigate the possibility of use as a probe for MRI. IO-BC-NAHis-GC nanoparticles were well observed in the PC3 cells, and the blocking with BBN significantly reduced the cellular binding of the nanoparticles.
Conclusion. These results demonstrate that the BBN conjugation to NAHis-GC nanoparticles improves their tumor accumulation in PC3-bearing mice in comparison to nanoparticles without BBN, suggesting that BC-NAHis-GC nanoparticles may be useful for prostate cancer imaging.

KEY WORDS: bombesin; imaging; magnetofluorescent nanoparticles; prostate cancer.

INTRODUCTION

Prostate cancer (PC) is one of the most common types of malignant tumor (1,2). In its early stages, PC rarely causes symptoms and the majority of men have no specific symptoms, resulting in late diagnoses. In general, the prognoses of men with localized cancer are excellent. However, once the cancer has spread to other organs, the prognosis of curing PC is poor. Thus, it is important to detect and treat PC while it is still asymptomatic. To improve the diagnostic sensitivity for early prostate cancer, attention has focused on the development of novel imaging strategies (3–5).

Polymer-based nanoparticles are a potential artificial nanostructure for medical applications, such as cancer detection, diagnosis and treatment, due to low toxicity and biodegradation, high drug- or gene-loading capacity, and water-solubility (6–9). Recently, polymer amphiphiles consisting of hydrophilic and hydrophobic moieties have received much attention in various biomedical fields, including drug and gene delivery, molecular imaging, and tissue engineering, because they spontaneously form nanostructures with hydrophobic cores and a hydrophilic outer shell in the aqueous phase (10–13). In particular, glycol chitosan (GC) with hydrophobic segments (such as deoxycholic acid, cholesterol, and cholanic acid) forms self-assembled nanoparticles in aqueous medium (14,15). The blood half-life of GC nanoparticles can prolong circulation time due to limited uptake into the liver and spleen caused by the hydrophilic outer shell (16,17). The prolonged circulation time *in vivo* allows the nanoparticles to extravasate and accumulate in tumor tissues, because the vascular architecture of tumors is disorganized due to rapid growth. The enhanced-permeability-and-retention (EPR) effect caused by the unique vascular structure of tumors may provide opportunities for tumor-targeted imaging and selective drug delivery on prolonged nanoparticles. GC nanoparticles show high tumor accumulation that is useful for *in vivo* delivery of anticancer drugs, peptides or genes by the EPR effect (18,19). Furthermore, the nanoparticle surface can be functionalized to enhance the efficiency of imaging and targeting (20). It has been demonstrated that the binding characteristics of nanoparticles can be improved by tagging target-specific ligands onto the nanoparticle surface (21,22).

[1] Department of Nuclear Medicine, Chonbuk National University Medical School and Hospital, 634-18, Geumam-2 dong, Dukjin-gu, Jeonju, Jeonbuk 561-712, Republic of Korea.
[2] Research Institute of Clinical Medicine, Chonbuk National University Medical School and Hospital, Jeonju, Jeonbuk 561-712, Republic of Korea.
[3] Cyclotron Research Center, Chonbuk National University Medical School and Hospital, Jeonju, Jeonbuk 561-712, Republic of Korea.
[4] To whom correspondence should be addressed. (e-mail: jayjeong@chonbuk.ac.kr)

Receptors that are uniquely overexpressed in tumors have been used as targets for cancer diagnosis and therapy. The gastrin-releasing peptide receptor (GRPR) is overexpressed in several human tumors, particular pancreatic cancer, prostate cancer and breast cancer (23). Bombesin (BBN) is a 14-amino-acid peptide that binds to members of the BBN receptor family, including the neuromedin B receptor, the GRPR, the orphan receptor subtype and the amphibian receptor. BBN and its analogues have been studied for diagnosis and therapy of GRPR-positive tumors (24–26). Therefore, it is expected that the tumor accumulation of GC nanoparticles in tumor-bearing mice may be improved by conjugation with BBN on the nanoparticle surface.

In this study, we investigated whether BBN conjugation improves the tumor accumulation of GC nanoparticles by the EPR effect in a prostate tumor model. The binding characteristics of BBN-conjugated GC nanoparticles were evaluated in PC3 cells *in vitro*. We also confirmed the improved tumor accumulation of BBN-conjugated GC nanoparticles in PC3-bearing mice through *in vivo* optical imaging studies. Further, we propose the possibility of BBN-conjugated GC nanoparticles loading iron oxide nanoparticles (IO) as a probe for magnetic resonance imaging (MRI) in prostate tumor-targeted imaging.

MATERIALS AND METHODS

Materials

Gycol chitosan (GC, Mw 250 KDa, degree of deacetylation 88.7%) was purchased from Wako Chemical Co. (Osaka, Japan). *N*-acetyl histidine (NAHis), *N*-hydroxysuccinimide (NHS), *N*-(3-dimethyl aminopropyl)-*N*′-ethylcarbodiimide hydrochloride (EDC) and 4′,6-diamidino-2-phenylindole (DAPI) were purchased from Sigma-Aldrich Chemical Co. (St. Louis, MO, USA). *N*-succinimidyl 3-(2-pyridyldithio) propionate (SPDP) was obtained from Pierce Co. (Rockford, IL, USA). Monoreactive hydroxysuccinimide ester of Cy5.5 (Cy5.5-NHS) was obtained from GE Healthcare (Uppsala, Sweden). Bombesin (BBN), CGGG-QWAVGHLM-NH_2(7–14) was synthesized using standard Fmoc chemistry by Peptron Inc. (Daejeon, South Korea). All other chemicals were of analytical grade and were used as received without further purification.

Cy5.5-Labeling and BBN Conjugation of NAHis-GC Conjugates

NAHis-GC conjugates were synthesized according to a previous method (26). GC (1 g) was dissolved in PBS, and NAHis (0.24 mmol) was added to the GC solution. EDC (0.72 mmol) and NHS (0.72 mmol) were added, and the reaction mixture was stirred for 24 h at room temperature. The reaction solution was dialyzed with a cellulose membrane (MWCO 12 KDa, Spectrum Laboratories, Rancho Dominguez, CA, USA) against distilled water for three days. The NAHis-GC conjugate was freeze-dried, and the NAHis content was analyzed by ^{1}H-NMR spectroscopy.

To label Cy5.5 to NAHis-GC conjugate, NAHis-GC (0.1 g) was dissolved in 50 ml of 0.05 M sodium borate buffer at pH 8.5. After adding Cy5.5-NHS solution in DMSO, the reaction mixture was stirred for 6 h at room temperature in the dark. The non-reacted Cy5.5-NHS was removed using a dialysis membrane with a molecular-weight cutoff of 12 KDa. The resulting NAHis-GC-Cy5.5 was lyophilized and stored at 4°C before use. BBN was conjugated to the NAHis-GC-Cy5.5 conjugate using SPDP as a bifunctional linker. SPDP (500 μg) in DMSO (20 μl) was added to the NAHis-GC-Cy5.5 solution in PBS (pH 7.4) with EDTA. After incubation for 3 h at room temperature, the SPDP-modified conjugate was filtered and washed to remove reaction byproducts and excess non-reacted SPDP in a centrifugal tube (cutoff 50 KDa, Falcon). BBN in water was added to the SPDP-modified conjugate solution, and the reaction mixture was incubated overnight at room temperature under dark. The final products were separated from non-reacted BBN and washed with a centrifugal Falcon tube. BBN-conjugated and Cy5.5-labeled NAHis-GC conjugate powders were obtained by freeze-drying.

Preparation and Morphological Characterization of BC-NAHis-GC Nanoparticles

Cy5.5-labeled NAHis-GC conjugate (5 mg) was suspended in 5 ml of PBS, and the suspension was sonicated for 10 min (the pulse was turned off for 1 s with an interval of 5 s) at 4°C using a probe-type sonicator (VCX 750 Ultrasonic Processor, Sonics & Materials, Inc., CT, USA) in the dark. The nanoparticle suspension was passed through a cellulose acetate syringe filter with 0.45-μm sized pores. The morphological features of the BBN-conjugated and Cy5.5-labeled NAHis GC (BC-NAHis-GC) nanoparticles were examined using transmission electron microscopy (TEM, JEOL, JEM-2010 located in the Center for Chonbuk National University-Wide Research Facilities). Atomic force microscopy (AFM) using a model of MultiMode™ (Digital Instruments, CA, USA) installed in KBSI (Jeonju, Korea) was also performed to characterize the surface morphology of the nanoparticles and to determine size distribution. The amount of BBN conjugated to the GC nanoparticles was determined using a BCA protein assay kit (Pierce, Rockford, IL, USA).

In Vitro Cell Binding Study

Human prostate cancer PC3 cells were incubated in RPMI-1640 culture medium with 10% fetal bovine serum. To evaluate the cell binding of BC-NAHis-GC nanoparticles, PC3 cells (1×10^5 cells/well) were seeded on glass cover slips in four-well plates at 37°C and then allowed to adhere to the plates overnight. The BC-NAHis-GC nanoparticle solution or C-NAHis-GC nanoparticle solution was added at a particle concentration of 100 μg/10 μl and incubated at 37°C for 1 h. Unbound nanoparticles were removed by washing with PBS (pH 7.4) three times. Cells were fixed with 4% (*w*/*v*) paraformaldehyde solution for 10 min and washed again. DAPI was added to stain the nuclei of the cells for 5 min at 37°C, and the cells were mounted in fluorescent mounting medium (Dako, Glostrup, Denmark). The slides were viewed using a Zeiss LSM 510 Meta confocal laser scanning microscope (Carl Zeiss Inc., Germany), and the fluorescence excitation used for imaging was 633 nm. Serial capture images were obtained at 1.5 μm intervals in the Z-direction. To investigate receptor-mediated specific binding, cells were co-treated with BC-NAHis-GC nanoparticles and BBN (25 nmol). To quantify cell binding, the cell slides were objected on an IVIS spectrum small-animal *in vivo* imaging

system (Caliper Lifescience, Hopkinton, MA, USA). The fluorescence images were obtained with the following settings: exposure time (1 s), f/stop (2), binning (8), and field of view (12.8). The excitation and emission filters were 640 nm and 700 nm, respectively. The fluorescence intensity for the cell binding was evaluated using Living Image software (Caliper Lifescience). *In vitro* binding affinity of the BC-NAHis-GC nanoparticles was determined using ^{125}I-[Tyr^4]BBN. The 50% inhibitory concentration (IC_{50}) value was calculated by fitting the data with nonlinear regression using Graph-Pad Prism (GraphPad Software, Inc.). Experiments were performed with triplicate samples.

In Vivo Optical Imaging Study

All animal experiments were performed according to the Institutional Animal Care and Use Committee for Animal Treatment of Chonbuk National University. Female athymic nude 4-week-old mice were obtained from Orient Bio, Inc. (Seoul, Korea). The mice were sedated by a subcutaneous injection of a mixture of ketamine (50 mg/kg body weight) and xylazine (10 mg/kg body weight). Tumor xenografts were prepared in the right flank by subcutaneous injection with 5×10^6 PC3 cells suspended in a mixture of 50 μl of PBS and 50 μl of Matrigel (BD Bioscience, San Jose, CA, USA). When the tumor implants reached 0.6 or 0.7 cm in diameter, optical imaging studies were performed using an IVIS spectrum small-animal *in vivo* imaging system (Caliper Lifescience, Hopkinton, MA). Mice bearing PC3 tumors were injected via tail vein with BC-NAHis-GC nanoparticles or C-NAHis-GC nanoparticles and imaged at 1, 3, and 6 h post-administration. Blood was drawn from tail vein of the mice for up to 3 h and analyzed by quantifying fluorescent intensity of the nanoparticle in the blood using an IVIS fluorescence imaging system. Isofluorane (2%) was used for anesthesia during imaging. The fluorescence images were obtained with the following settings: exposure time (1 s), f/stop (2), binning (8) and field of view (12.8). Excitation filters were 640, 604, and 570 nm, and the emission filter was 700 nm. All images were background subtracted using Living Image software. Tumor, heart, lung, liver, spleen, pancreas, muscle, and bone were dissected from mice 6 h post-injection, and the dissected tissues were imaged immediately. The mean fluorescence intensity of the tumor and muscle was calculated using Living Image software.

Loading of Iron Oxide Nanoparticle and Cell Binding Assay

BC-NAHis-GC conjugates (10 mg) were dissolved in 10 ml of PBS (pH 7.4) and sonicated for 5 min at 4°C. The synthesis of iron oxide nanoparticles (IO) decorated with oleic acid and oleylamine has been previously reported in our paper (7). IO solution (1 mg/ml in chloroform) was added to the BC-NAHis-GC nanoparticle solution, and the mixture was sonicated for 10 min in an ice-water bath. To completely evaporate the organic solvent, the resulting solution was stirred for 12 h at room temperature. Iron loaded in the BC-NAHis-GC nanoparticles was quantified according to a previously reported method (7). The morphology of the IO nanoparticle-loaded BC-NAHis-GC (IO-BC-NAHis-GC) nanoparticles was determined by TEM (JEOL, JEM-2010 located in Center for Chonbuk National University-Wide Research Facilities). The PC3 cell-binding studies for IO-BC-NAHis-GC nanoparticles were performed according to the previously described method. The binding of IO-BC-NAHis-GC nanoparticles was identified by

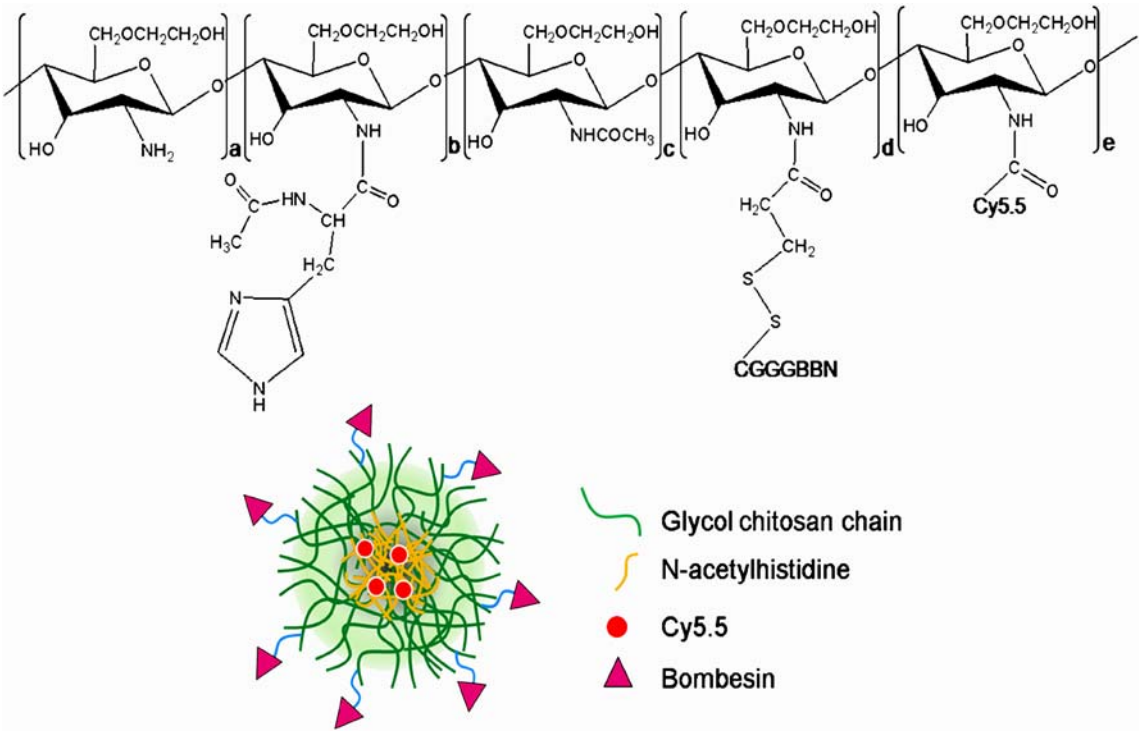

Fig. 1. Chemical structures of *NAHis-GC conjugates labeled with Cy5.5 and tagged with BBN. A diagram of **BC-NAHis-GC nanoparticles is shown below. **NAHis-GC conjugates = N-acetylhistidine-glycol chitosan conjugates, **BC-NAHis-GC nanoparticles = BBN-conjugated and Cy5.5-labled NAHis-GC nanoparticles.*

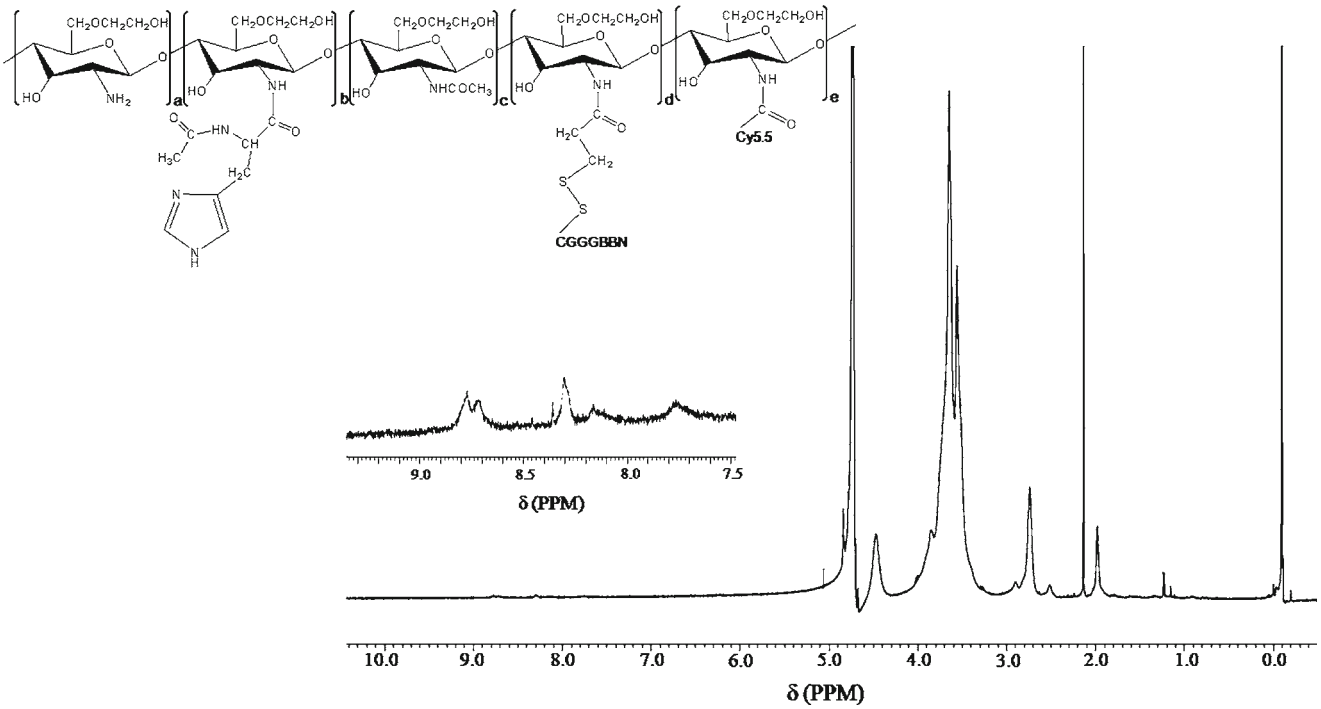

Fig. 2. ^{1}H-NMR spectrum of BC-NAHis-GC nanoparticles in D_2O.

Prussian blue staining. All micrographs were obtained using a light microscope with a digital camera.

Statistical Analysis

Quantitative data were expressed as the mean ± SD. Means were compared by use of an independent samples *T* test. *P* values of less than 0.05 were considered statistically significant.

RESULTS AND DISCUSSION

Synthesis and Characterization of BC-NAHis-GC Nanoparticles

A schematic diagram of BC-NAHis-GC nanoparticles is shown in Fig. 1. To form self-assembled nanoparticles, amphiphilic NAHis-GC conjugate was synthesized through formation of an amide bond according to a previously reported method (27). The NAHis content of the conjugates

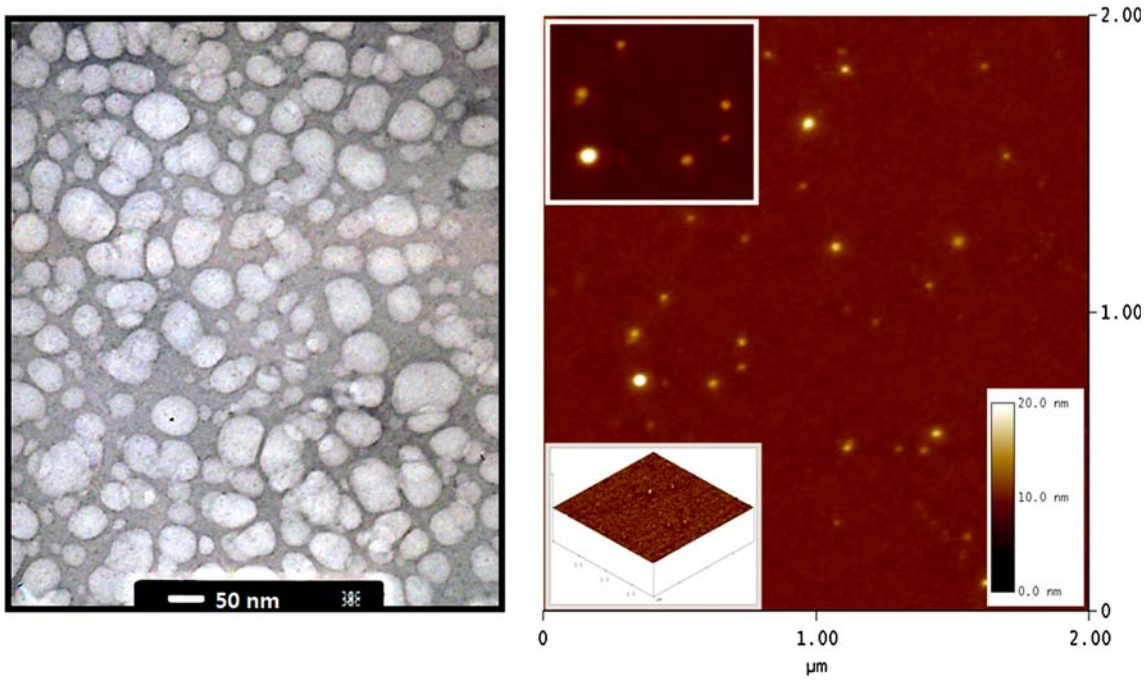

Fig. 3. Transmission electron microscopic image (**A**) and atomic force microscopic image (**B**) of BC-NAHis-GC nanoparticles.

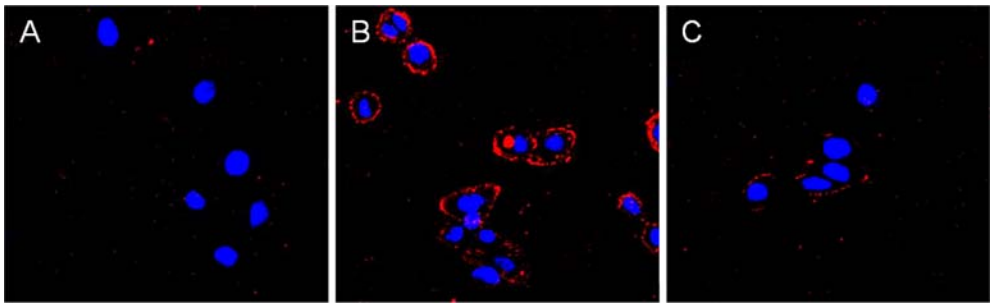

Fig. 4. Confocal images of PC3 cells. The images of PC3 cells were obtained after incubation for 1 h in the presence of *C-NAHis-GC (**A**) and BC-NAHis-GC nanoparticles without (**B**) or with (**C**) blocking with BBN. The cellular uptake of BC-NAHis-GC nanoparticles was reduced by BBN. The nuclei of the cells were stained using DAPI (*blue*). **C-NAHis-GC = Cy5.5-labeled NAHis-GC nanoparticles.*

was measured by ^{1}H-NMR spectroscopy, and the degree of substitution of NAHis per 100 sugar residues of GC was 6.5. The proton assignment in the aromatic region of BBN and Cy5.5 was observed in the range of 7.5–9.0 ppm (Fig. 2). Furthermore, the proton signal of methyl groups of BBN and Cy5.5 was characterized at 1.20 ppm (28). The molar ratio of Cy5.5 conjugated to NAHis-GC conjugate was 2.5, as determined by fluorescence spectrometry. To conjugate BBN on to the NAHis-GC nanoparticles, we used a bifunctional SPDP as a linker. BBN was conjugated with 1.3 wt-% on the NAHis-GC nanoparticles. When the conjugate was dispersed in water and sonicated, BBN- and Cy5.5-conjugated NAHis-GC conjugate formed self-assembled nanoparticles with spherical morphology. Their morphology was determined by TEM and AFM (Fig. 3). The diameter of the BC-NAHis-GC nanoparticles was determined by AFM and ranged from 35 nm to 97 nm.

In Vitro Binding of BC-NAHis-GC Nanoparticles to PC3 Cells

The specific binding of BC-NAHis-GC nanoparticles to BBN-positive PC3 cells was measured by confocal fluorescent microscopy. To conduct a competitive binding assay, BBN was treated with BC-NAHis-GC nanoparticle on PC3 cells. Fig. 4 shows the fluorescent microscopic images of PC3 cells incubated with BC-NAHis-GC nanoparticles, C-NAHis-GC nanoparticles or BBN plus BC-NAHis-GC nanoparticles. Cellular nuclei were stained with DAPI. BC-NAHis-GC nanoparticles were found mainly on the cell surfaces of the PC3 cells, whereas there was no significant binding of the C-NAHis-GC nanoparticles (Fig. 4A and C). Fig. 4C demonstrates that blocking the GRPR with BBN reduces the binding affinity of the BC-NAHis-GC nanoparticles. These results clearly indicate that the binding of BC-NAHis-GC nanoparticles is specifically mediated by the receptor related to BBN. To examine the binding sites of BC-NAHis-GC nanoparticles on PC3 cells, we obtained sliced fluorescence images at 1.5 μm-depth intervals (Fig. 5). The resulting images demonstrated that most of BC-NAHis-GC nanoparticles bound to the cell membrane. Some nanoparticles were also found in the cell cytoplasm due to non-specific cellular binding. GRPR has been isolated from various tumors, including prostate tumors. BBN and BBN-like peptides are endocytosed following binding to the receptors present on the cell surface (23,29).

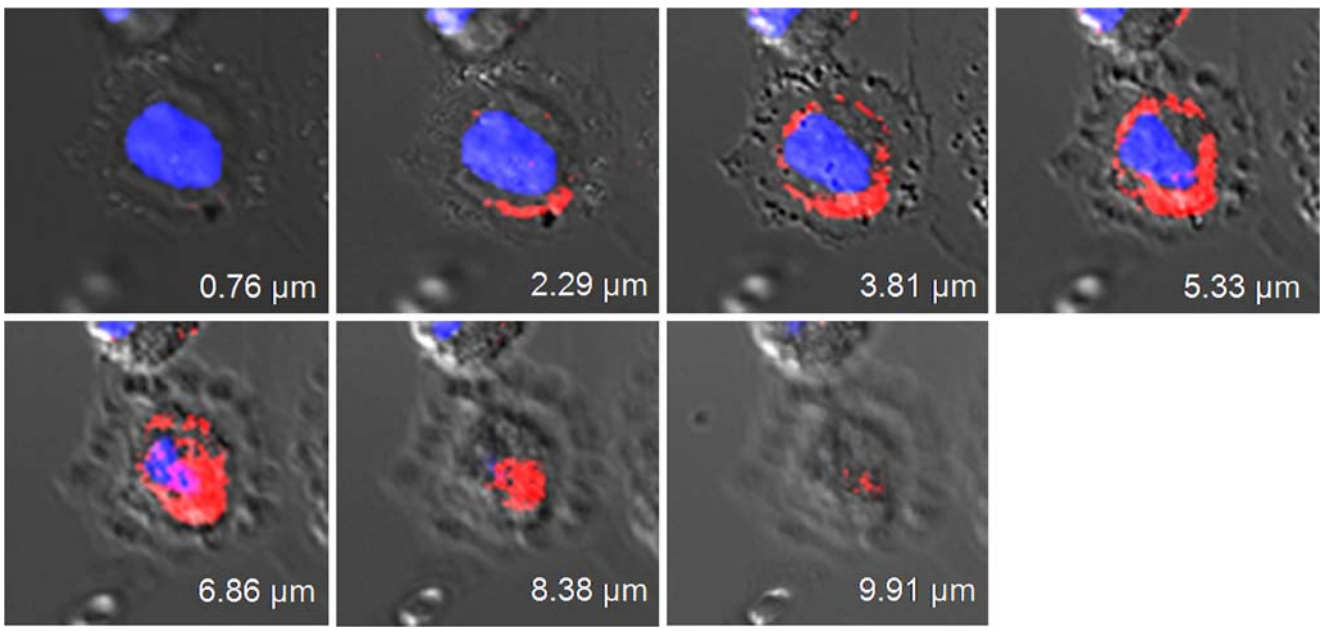

Fig. 5. Confocal serial Z-section images of PC3 cells incubated with BC-NAHis-GC nanoparticles (100 μg/ml, 1 h). The *image* indicates that most nanoparticles were bound to the membranes of PC3 cells.

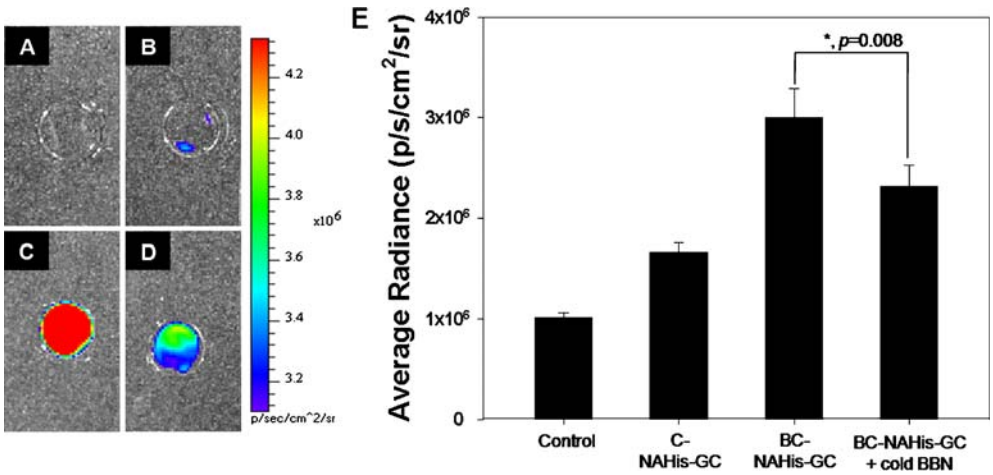

Fig. 6. *In vitro* NIR imaging for quantification of cellular uptake. These images were obtained from PC3 cells incubated in the absence (**A**) or the presence of C-NAHis-GC (**B**) or BC-NAHis-GC nanoparticles without (**C**) or with (**D**) blocking with BBN. The quantitative analyses (**E**) of cellular uptake were calculated using the average radiance values of ROI and IVIS imaging software. This result shows that BC-NAHis-GC nanoparticles bind specifically to the PC3 cells. The data represent the mean ± SD (n=4).

Additionally, the quantification results for cellular binding of the nanoparticles using an IVIS imaging system and its image software are shown in Fig. 6. Cellular binding of the BC-NAHis-GC nanoparticles had a higher average radiance value than that of the C-NAHis-GC nanoparticles. After blocking with BBN, the binding of BC-NAHis-GC to PC3 cells was significantly inhibited compared to that of the BC-NAHis-GC nanoparticles without blocking, which indicates that BC-NAHis-GC nanoparticles are specifically bound to their receptor on the cells. The binding affinity of the BC-NAHis-GC nanoparticles was evaluated for PC3 cells using ^{125}I-[Tyr^4]BBN as a radioligand (Fig. 7). The IC50 value of the BC-NAHis-GC nanoparticles was determined to be 4.3×10^{-2} μg/μL.

In Vivo Optical Imaging

The targetability of the BC-NAHis-GC nanoparticle for PC3 tumors was assessed *in vivo* using an IVIS *in vivo* imaging system. Fig. 8 shows the near infrared images of mice bearing PC3 tumors 1, 3 and 6 h after intravenous injection of C-NAHis-GC or BC-NAHis-GC nanoparticles. BC-NAHis-GC nanoparticles exhibited a higher signal in the area surrounding the tumor compared to the C-NAHis-GC nanoparticles. The fluorescence intensity observed in the tumors for BC-NAHis-GC nanoparticles increased with time. In contrast, C-NAHis-GC nanoparticles exhibited no difference in the intensity from the tumors during 6 h. This result indicates that tumoral uptake in a relatively short time after injection was improved by conjugation of BBN on the NAHis-GC nanoparticles. To characterize the biodistribution of C- and BC-NAHis-GC nanoparticles, the mice bearing PC3 tumors were sacrificed 6 h post-injection after *in vivo* imaging and *ex vivo* imaging for selected organs was performed. The fluorescent signal from the accumulation of C- and BC-NAHis-GC nanoparticles was mainly observed in the liver, kidney and tumor. The tumor-to-muscle (T/M) ratios are shown in Fig. 9. The T/M ratios for C- and BC-NAHis-GC nanoparticles were 2.26±0.66 and 5.37±0.43, respectively. To further characterize the specific uptake by receptor mediation, *ex vivo* imaging was accomplished after co-injection of BBN, with BC-NAHis-GC nanoparticles into the tumor-bearing mice. The tumor fluorescence intensity was clearly reduced by BBN, and the T/M ratio was 3.88±0.54. We suggest that C-NAHis-GC nanoparticles show little tumor accumulation as early as 6 h due to their prolonged circulation in bloodstream (30,31). These results imply that BC-NAHis-GC nanoparticles may selectively bind to GRPR-expressing tissues *in vivo* and show higher accumulation in the tumors within 6 h after injection than C-NAHis-GC nanoparticles without BBN.

Blood Circulation of Nanoparticles

To characterize the blood circulation of C- and BC-NAHis-GC nanoparticles, we determined the fluorescence intensity in the blood of mice at 3 h. Fig. 10 shows the change in fluorescence intensity in the blood after injection of the nanoparticles. Half of the BC-NAHis-GC nanoparticles were rapidly cleared from the blood within 15 min, whereas 63% of the injected C-NAHis-GC nanoparticles remained in the blood for up to 3 h. These results indicate that BC-NAHis-GC nanoparticles are rapidly cleared from the bloodstream, whereas NAHis-GC nanoparticles without BBN have a relatively prolonged blood circulation profile after systemic injection.

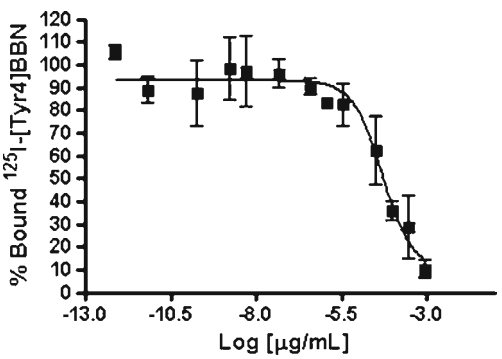

Fig. 7. Inhibition of ^{125}I-[Tyr^4]BBN binding on PC3 cells by BC-NAHis-GC nanoparticles (n=3, mean ± SD).

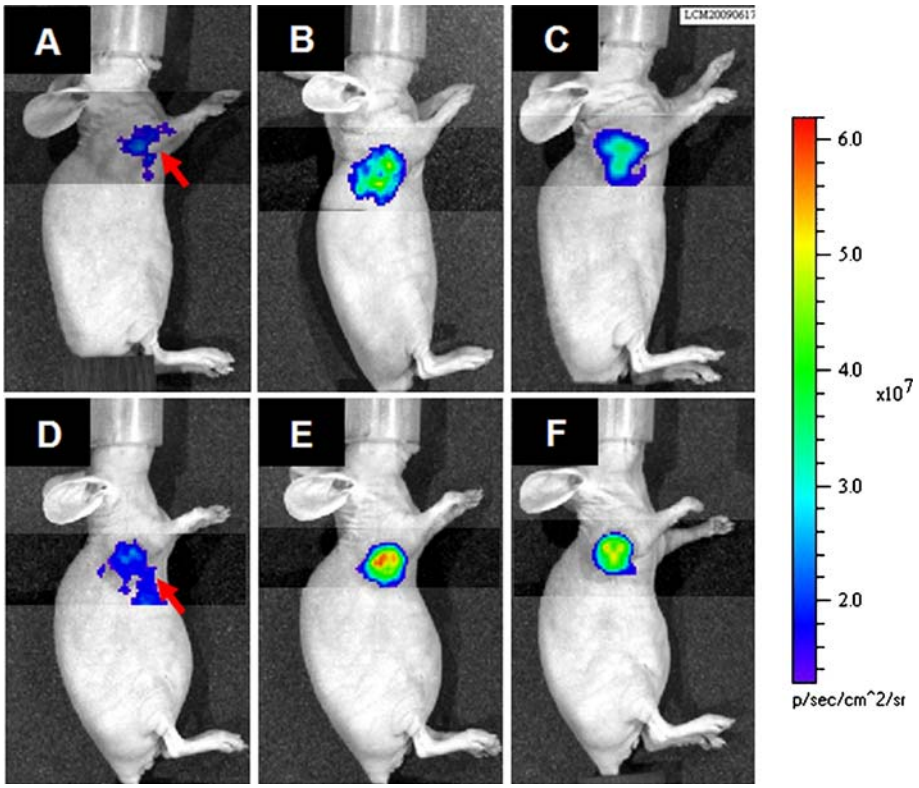

Fig. 8. *In vivo* non-invasive NIF images of athymic nude mice with PC3 tumors. Images from mice after injection of C-NAHis-GC (**A**–**C**) or BC-NAHis-GC (**D**–**E**) nanoparticles at 1 h (**A** and **D**), 3 h (**B** and **E**) and 6 h (**C** and **F**), with the background fluorescence subtracted. The *solid red arrows* indicate the tumors.

Many researchers have reported that hydrophobically modified GC nanoparticles show a prolonged blood circulation profile after intravenous injection *in vivo* and that they preferentially accumulate in tumors in animal models (32–34). The accumulation of nanoparticles in tumors increased for up to 2 or 3 days and was maintained for up to 5 days (32,33). The blood circulation time of the nanoparticles may be reduced, and their targetability may be increased by conjugation of peptides or antibodies as target ligands, because peptides or antibodies on the surface of the nanoparticles generally enhance the multivalent attachment to various cells that are expressing the targeted receptors (20,35). BBN on the surface of NAHis-GC nanoparticles offers good binding selectivity to GRPR-expressing tumors *in vivo*. These results indicate that shortly after intravenous injection *in vivo*, BBN-NAHis-GC nanoparticles may be more useful for detecting tumors than NAHis-GC nanoparticles without BBN.

IO Nanoparticle Loading and Cellular Binding

To assess magnetic resonance imaging (MRI), IO nanoparticles were loaded into BC-NAHis-GC nanoparticles (IO-

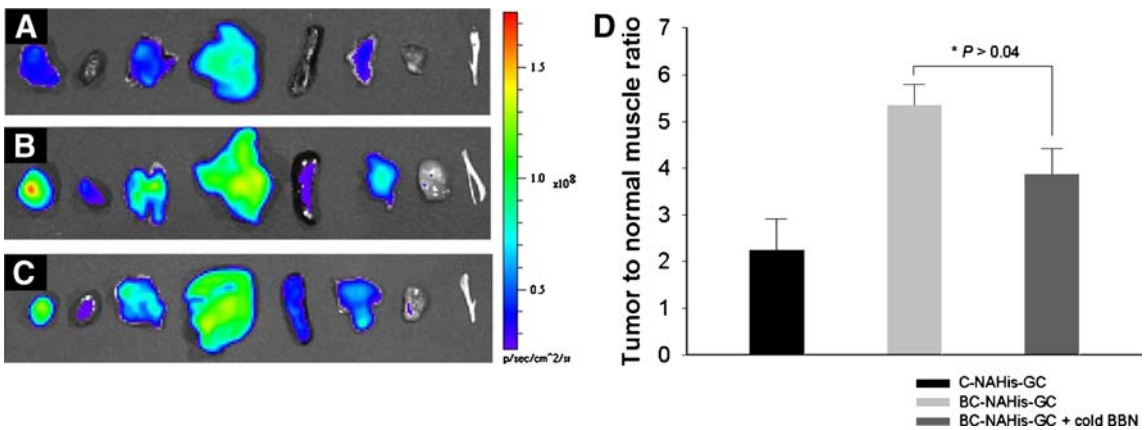

Fig. 9. *Ex vivo* NIF imaging of tissues (from *left to right*; tumor, heart, lung, liver, spleen, pancreas, muscle, and bone) collected from PC3-bearing mice at 6 h after injection of C-NAHis-GC (**A**) or BC-NAHis-GC nanoparticles without (**B**) or with (**C**) blocking with BBN. A quantification of tumor to normal muscle ratios (**D**) was calculated using the average radiance values of the tissue signal intensity. All data represent the mean ± SD (n=3).

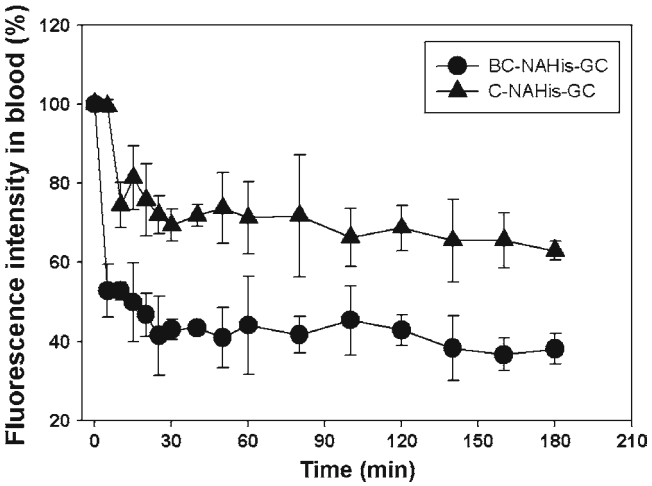

Fig. 10. Changes in the fluorescence intensity of blood of mice after i.v. injection of C-NAHis-GC (●) or BC-NAHis-GC (▲) nanoparticles. All data represent the mean ± SD (n=3).

BC-NANis-GC nanoparticles), and their cellular binding affinities were investigated *in vitro*. Hydrophobic IO nanoparticles capped with oleic acid and oleylamine were synthesized according to a previously reported method (7). We previously reported that the IO nanoparticles exhibit superparamagnetic properties and show a narrow distribution with a 12 nm mean diameter (7,8). As shown in Fig. 11A and B, hydrophobic IO nanoparticles could be loaded into BC-NAHis-GC nanoparticles by hydrophobic interaction between oleic acid of IO nanoparticles and NAHis core of BC-NAHis-GC nanoparticles. The clustering of IO nanoparticles inside BC-NAHis-GC nanoparticles was clearly observed. The IO nanoparticle clusters may allow the dramatic increase of T_2 relaxitivity (36). The diameters of IO-BC-NAHis-GC nanoparticles ranged from 45 nm to 90 nm. After IO loading, there were no significant diameter differences between IO- *versus* BC-NAHis-GC nanoparticles. The loading efficiency of IO nanoparticles inside BC-NAHis-GC nanoparticles was 87% (*w*/*w*). The targeting specificity of IO-BC-NAHis-GC nanoparticles was investigated by measuring the cellular binding in comparison to IO-C-NAHis-GC nanoparticles and by blocking using BBN. The binding of nanoparticles was visualized by a Prussian blue staining assay. The cellular binding of IO-BC-NAHis-GC nanoparticles was clearly observed with blue dots (Fig. 11D). In comparison, blocking with BBN significantly reduced the number of blue dots (Fig. 11E). These results indicate that BC-NAHis-GC nanoparticles are specifically bound to PC3 cells after the loading of IO nanoparticles. Further, the results imply that IO-BC-NAHis-GC nanoparticles may be useful for targeted MR imaging.

CONCLUSION

In this study, we designed magnetofluorescent polymeric nanoparticles for targeted imaging of prostate cancer. *In vitro* confocal microscopy and IVIS imaging studies showed that BBN-conjugated NAHis-GC nanoparticles selectively bind to GRPR-overexpressing prostate cancer cells. After IO load-

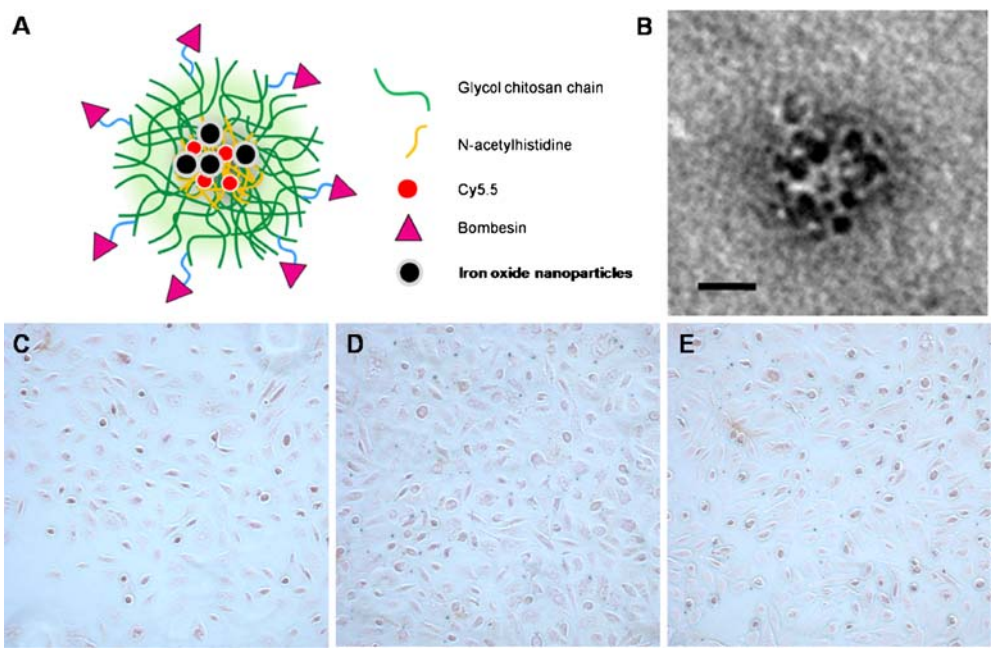

Fig. 11. Schematic illustration (**A**) and TEM image (**B**) of *IO-BC-NAHis-GC nanoparticles. The *scale bar* indicates 50 nm. The microscopic images of PC3 cells stained after incubation for 1 h in the presence of **IO-C-NAHis-GC (**C**) or IO-BC-NAHis-GC nanoparticles without (**D**) or with (**E**) blocking with BBN. The *blue dots* indicate the presence of IO. The magnification is 200 times. This result shows that IO-BC-NAHis-GC nanoparticles selectively bind to PC3 cells. **IO-BC-NAHis-GC nanoparticles* = *Iron oxide nanoparticles-loaded BC-NAHis-GC nanoparticles,* ***IO-C-NAHis-GC nanoparticles* = *Iron oxide nanoparticles-loaded C-NAHis-GC nanoparticles.*

ing, BBN-conjugated NAHis-GC nanoparticles demonstrated superior binding to PC3 cells than NAHis-GC nanoparticles without BBN. In animal optical imaging studies, BBN-conjugated NAHis-GC nanoparticles exhibited a higher fluorescent signal in the tumor lesion compared to the NAHis-GC nanoparticles without BBN. The tumor accumulation of BBN-conjugated NAHis-GC nanoparticles was clearly inhibited by blocking with BBN *in vivo*. Therefore, we conclude that BBN-conjugated NAHis-GC nanoparticles are useful as a probe for prostate cancer imaging.

ACKNOWLEDGMENTS

This study was supported by a grant from the National R&D Program for Cancer Control, Ministry of Health, Welfare and Family Affairs, Republic of Korea (0620220 and 0720420). This work was also supported by the Nuclear R&D Program through the Korea Science and Engineering Foundation funded by the Ministry of Science & Technology (contract grant numbers: 20090062447).

REFERENCES

1. Franiel T, Lüdemann L, Rudolph B, Rehbein H, Stephan C, Taupitz M, *et al*. Prostate MR imaging: tissue characterization with pharmacokinetic volume and blood flow parameters and correlation with histologic parameters. Radiology. 2009;252:101–8.
2. Zaheer A, Cho SY, Pomper MG. New agents and techniques for imaging prostate cancer. J Nucl Med. 2009;50:1387–90.
3. Kelly KA, Setlur SR, Ross R, Anbazhagan R, Waterman P, Rubin MA, *et al*. Detection of early prostate cancer using a hepsin-targeted imaging agent. Cancer Res. 2008;68:2286–91.
4. LeBeau AM, Banerjee SR, Pomper MG, Mease RC, Denmeade SR. Optimization of peptide-based inhibitors of prostate-specific antigen (PSA) as target imaging agents for prostate cancer. Bioorg Med Chem. 2009;17:4888–93.
5. Schroeder RPJ, van Weerden WM, Bangma C, Krenning EP, de Jong M. Peptide receptor imaging of prostate cancer with radiolabelled bombesin analogues. Methods. 2009;48:200–4.
6. Lee SJ, Park K, Oh YK, Kwon SH, Her S, Kim IS, *et al*. Tumor specificity and therapeutic efficacy of photosensitizer-encapsulated glycol chitosan-based nanoparticles in tumor-bearing mice. Biomaterials. 2009;30:2929–39.
7. Lee CM, Jeong HJ, Kim SL, Kim EM, Kim DW, Lim ST, *et al*. SPION-loaded chitosan-linoleic acid nanoparticles to target hepatocytes. Int J Pharm. 2009;371:163–9.
8. Cheong SJ, Lee CM, Kim SL, Jeong HJ, Kim EM, Park EH, *et al*. Superparamagnetic iron oxide nanoparticles-loaded chitosan-linoleic acid nanoparticles as an effective hepatocyte-targeted gene delivery system. Int J Pharm. 2009;372:169–76.
9. Lee CM, Jeong HJ, Park JW, Kim J, Lee KY. Temperature-induced release of all-trans-retinoic acid loaded in solid lipid nanoparticles for topical delivery. Macromol Res. 2008;16:682–5.
10. Kim JH, Kim YS, Park K, Lee S, Nam HY, Min KH, *et al*. Antitumor efficacy of cisplatin-loaded glycol chitosan nanoparticles in tumor-bearing mice. J Control Release. 2008;127:41–9.
11. Liu L, Xu K, Wang H, Tan PK, Fan W, Venkatraman SS, *et al*. Self-assembled cationic peptide nanoparticles as an efficient antimicrobial agent. Nat Nanotechnol. 2009;4:457–63.
12. Papadimitriou S, Bikiaris D. Novel self-assembled core-shell nanoparticles based on crystalline amorphous moieties of aliphatic copolyesters for efficient controlled drug release. J Control Release. 2009;138:177–84.
13. Park JH, Kwon S, Nam JO, Park RW, Chung H, Seo SB, *et al*. Self-assembled nanoparticles based on glycol chitosan bearing 5beta-cholanic acid for RGD peptide delivery. J Control Release. 2004;95:579–88.
14. Yu JM, Li YJ, Qiu LY, Jin Y. Polymeric nanoparticles of cholesterol-modified glycol chitosan for doxorubicin delivery: preparation and *in-vitro* and *in-vivo* characterization. J Pharm Pharmacol. 2009;61:713–9.
15. Min KH, Park K, Kim YS, Bae SM, Lee S, Jo HG, *et al*. Hydrophobically modified glycol chitosan nanoparticles-encapsulated camptothecin enhance the drug stability and tumor targeting in cancer therapy. J Control Release. 2008;127:208–18.
16. Park JH, Kwon S, Lee M, Chung H, Kim JH, Kim YS, *et al*. Self-assembled nanoparticles based on glycol chitosan bearing hydrophobic moieties as carriers for doxorubicin: *in vivo* biodistribution and anti-tumor activity. Biomaterials. 2006;27:119–26.
17. Youn H, Kang KW, Chung JK, Lee DS. Nanomedicine: drug delivery systems and nanoparticle targeting. Nucl Med Mol Imaging. 2008;42:337–46.
18. Hwang HY, Kim IS, Kwon IC, Kim YH. Tumor targetability and antitumor effect of docetaxel-loaded hydrophobically modified glycol chitosan nanoparticles. J Control Release. 2008;128:23–31.
19. Kim JH, Kim YS, Park K, Kang E, Lee S, Nam HY, *et al*. Self-assembled glycol chitosan nanoparticles for the sustained and prolonged delivery of antiangiogenic small peptide drugs in cancer therapy. J Control Release. 2008;29:1920–30.
20. Park K, Hong HY, Moon HJ, Lee BH, Kim IS, Kwon IC, *et al*. A new atherosclerotic lesion probe based on hydrophobically modified chitosan nanoparticles functionalized by the atherosclerotic plaque targeted peptides. J Control Release. 2008;128:217–23.
21. Riehemann K, Schneider SW, Luger TA, Godin B, Ferrari M, Fuchs H. Nanomedicine—challenge and perspectives. Angew Chem Int Ed. 2009;48:872–97.
22. Sun C, Veiseh O, Gunn J, Fang C, Hansen S, Lee D, *et al*. *In vivo* MRI detection of gliomas by chlorotoxin-conjugated superparamagnetic nanoprobes. Small. 2008;4:372–9.
23. Varvarqou A, Bouziotis P, Zikos C, Scopinaro F, de Vincentis C. Gastrin-releasing peptide (GRP) analogues for cancer imaging. Cancer Biother Radiopharm. 2004;19:219–29.
24. Ananias HJ, de Jong IJ, Dierckx RA, van de Wiele C, Helfrich W, Elsinqa PH. Nuclear imaging of prostate cancer with gastrin-releasing-peptide-receptor targeted radiopharmaceuticals. Curr Pharm Des. 2008;14:3033–47.
25. Rogers BE, Zinn KR, Buchsbaum DJ. Gene transfer strategies for improving radiolabeled peptide imaging and therapy. Q J Nucl Med. 2000;44:208–23.
26. Safavy A, Khazaeli MB, Qin H, Buchsbaum DJ. Synthesis of bombesin analogues for radiolabeling with rhenium-188. Cancer. 1997;80:2354–9.
27. Park JS, Han TH, Lee KY, Han SS, Hwang JJ, Moon DH, *et al*. N-acetyl histidine-conjugated glycol chitosan self-assembled nanoparticles for intracytoplasmic delivery of drugs: endocytosis, exocytosis and drug release. J Control Release. 2006;115:37–45.
28. Saravanakumar G, Min KH, Min DS, Kim AY, Lee CM, Cho YW, *et al*. Hydrotropic oligomer-conjugated glycol chitosan as a carrier of paclitaxel: synthesis, characterization, and *in vivo* biodistribution. J Control Release. 2009;140:210–7.
29. Van de Wiele C, Dumont F, Van Belle S, Slegers G, Peers SH, Dierckx RA. Is there a role for agonist gastrin-releasing peptide receptor radioligands in tumor imaging? Nucl Med Commun. 2001;22:5–15.
30. Lee SJ, Park K, Oh YK, Kwon SH, Her S, Kim IS, *et al*. Tumor specificity and therapeutic efficacy of photosensitizer-encapsulated glycol chitosan-based nanoparticles in tumor-bearing mice. Biomaterials. 2009;30:2929–39.
31. Jo HG, Min KH, Nam TH, Na SJ, Park JH, Jeong SY. Prolonged antidiabetic effect of zinc-crystallized insulin loaded glycol chitosan nanoparticles in type 1 diabetic rats. Arch Pharm Res. 2008;31:918–23.
32. Cho YW, Park SA, Han TH, Son DH, Park JS, Oh SJ, *et al*. *In vivo* tumor targeting and radionuclide imaging with self-assembled nanoparticles: mechanisms, key factors, and their implications. Biomaterials. 2007;28:1236–47.

33. Park K, Kim JH, Nam YS, Lee S, Nam HY, Kim K, *et al*. Effect of polymer molecular weight on the tumor targeting characteristics of self-assembled glycol chitosan nanoparticles. J Control Release. 2007;122:305–14.
34. Kim JH, Kin YS, Kim S, Park JH, Kim K, Choi K, *et al*. Hydrophobically modified glycol chitosan nanoparticles as carriers for paclitaxel. J Control Release. 2006;111:228–34.
35. Jiang HL, Kwon JT, Kim EM, Kim YK, Arote R, Jere D, *et al*. Galactosylated poly(ethylene glycol)-chitosan-graft-polyethylenimine as a gene carrier for hepatocyte-targeting. J Control Release. 2008;131:150–7.
36. Nasongkla N, Bey E, Ren J, Ai H, Khemtong C, Guthi JS, *et al*. Multifunctional polymeric micelles as cancer-targeted, MRI-ultrasensitive drug delivery systems. Nano Lett. 2006;6:2427–30.